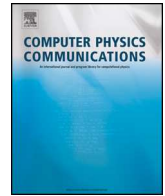




Contents lists available at ScienceDirect

Computer Physics Communications

www.elsevier.com/locate/cpc



BORAY: A ray tracing code for various magnetized plasma configurations ☆, ☆☆

Hua-sheng Xie ^{a,b}, Debabrata Banerjee ^{a,b}, Yu-kun Bai ^{a,b}, Han-yue Zhao ^{a,b}, Jing-chun Li ^c

^a Hebei Key Laboratory of Compact Fusion, Langfang 065001, China

^b ENN Science and Technology Development Co., Ltd., Langfang 065001, China

^c Department of Earth and Space Sciences, Southern University of Science and Technology, Shenzhen 518055, China

ARTICLE INFO

Article history:

Received 26 May 2021

Received in revised form 13 March 2022

Accepted 25 March 2022

Available online xxxx

Dataset link: [10.17632/tnkrjdbcz8.1](https://doi.org/10.17632/tnkrjdbcz8.1)

Keywords:

Plasma waves

Ray tracing

Cold plasma dispersion relation

Kinetic plasma dispersion relation

ABSTRACT

Ray tracing codes are useful to study the electromagnetic wave propagation and absorption in the geometrical optics approximation. In magnetized fusion plasma community, most ray tracing codes assume the plasma density and temperature be functions of the magnetic flux and study waves only inside the last closed flux surface, which are sufficient for the present day tokamak. However, they are difficult to be used for configurations with open magnetic field line plasmas, such as mirror machine and field-reversed-configuration (FRC). We develop a ray tracing code in cylindrical coordinates (r, ϕ, z) to support arbitrary axisymmetric configurations with both closed and open field lines plasmas. For wave propagation, the cold plasma dispersion relation is usually sufficient, and we require the magnetic field $\mathbf{B}(r, z)$ and species densities $n_{s0}(r, z)$ profiles as input. For wave absorption, we require a further temperature $T_{s0}(r, z)$ profile to solve a hot kinetic plasma dispersion relation. In difference to other ray tracing codes which calculate the imaginary part of wave vector $\mathbf{k}_{\perp, i}$ for wave absorption, we calculate the imaginary part of wave frequency ω_i , which is shown to be equivalent with the former technique under weak damping approximation. The code can use either numerical or analytical equilibrium. Examples and benchmarks with electron cyclotron wave, lower hybrid wave and ion cyclotron wave for tokamak, spherical tokamak (ST), FRC and mirror machine are shown.

Program summary

Program Title: BORAY

CPC Library link to program files: <https://doi.org/10.17632/tnkrjdbcz8.1>

Code Ocean capsule: <https://codeocean.com/capsule/6205646>

Licensing provisions: BSD 3-clause

Programming language: Matlab

Nature of problem: Solve the plasmas electromagnetic wave propagation and absorption in the geometrical optics approximation for magnetized plasmas based on ray tracing of plasma dispersion relation. In axisymmetric (r, z) coordinates, the code can be used for both closed and open field lines plasmas of various configurations such as tokamak, spherical tokamak, FRC and mirror machine.

Solution method: Runge-Kutta time integral to solve ray tracing equations for wave propagation, and integral the imaginary part of the wave frequency in hot kinetic dispersion relation for wave absorption.

Additional comments including restrictions and unusual features: Kinetic relativistic effects and collisional damping are not included in the present version yet. Only axisymmetric two-dimensional (2D) profiles are support in present version.

© 2022 Elsevier B.V. All rights reserved.

☆ The review of this paper was arranged by Prof. W. Walker.

☆☆ This paper and its associated computer program are available via the Computer Physics Communications homepage on ScienceDirect (<http://www.sciencedirect.com/science/journal/00104655>).

E-mail addresses: huashengxie@gmail.com, xiehuasheng@enn.cn (H.-s. Xie).

<https://doi.org/10.1016/j.cpc.2022.108363>

0010-4655/© 2022 Elsevier B.V. All rights reserved.

1. Introduction

In magnetic confinement plasmas, wave heating is one of the most important approach to heating the plasma to high temperature (>10 keV). The usually used waves from high frequency (~ 100 GHz) to low frequency (<1 MHz) include electron cyclotron

1 wave (ECW), lower hybrid wave (LHW), ion cyclotron wave (ICW)
2 and Alfvén wave (AW). There are also terminologies such as fast
3 wave (FW), slow wave (SW), helicon wave, etc. A simple but still
4 accurate way to study the wave propagation and heating is using
5 the geometrical optics approximation, which yields the ray tracing
6 equations.

7 The ray tracing equations in Cartesian coordinates are

$$8 \frac{d\mathbf{r}}{dt} = \frac{\partial \omega}{\partial \mathbf{k}} = -\frac{\partial D/\partial \mathbf{k}}{\partial D/\partial \omega} = \mathbf{v}_g, \quad (1)$$

$$9 \frac{d\mathbf{k}}{dt} = -\frac{\partial \omega}{\partial \mathbf{r}} = \frac{\partial D/\partial \mathbf{r}}{\partial D/\partial \omega}, \quad (2)$$

10 with the dispersion relation

$$11 D(\omega, \mathbf{k}, \mathbf{r}) = 0, \quad (3)$$

12 where ray position $\mathbf{r} = (x, y, z)$ and wave vector $\mathbf{k} = (k_x, k_y, k_z)$.
13 Here, ω is wave frequency, and \mathbf{v}_g is wave group velocity. The
14 geometrical optics approximation is valid in cases where the wave
15 length is much smaller than the system nonuniform length, which
16 is usually well satisfied for high frequency waves such as ECW and
17 LHW, but should be used with caution for low frequency waves
18 such as ICW and AW.

19 Several widely used ray tracing codes are available in magnetic
20 confinement fusion community, such as GENRAY [4], TORAY [6],
21 C3PO [5], CURRAY [8] and TASK/WR [10]. However, most of them
22 are developed for tokamak and use single fluid magnetohydro-
23 dynamics (MHD) equilibrium, thus the density and temperature
24 profiles are set to be magnetic flux functions, and the open field
25 line region is either omitted or simplified. The assumption that the
26 density and temperature profiles be flux functions is helpful to ob-
27 tain the flux average power absorption and to calculate the driven
28 current. These treatments can be useful and sufficient for studying
29 the present day tokamak. However, they can not be used to the
30 configurations with open field line plasmas or when the density
31 and temperature are not magnetic flux functions. There are also
32 codes for some special cases such as RAYS [7] (which is later up-
33 dated to TORAY) for mirror configuration and FRTC [9] for LHW. In
34 Ref. [15], a simplified model is used to study the ECRH in mirror.
35 Thus the need for relaxing these restrictions in order to make a
36 code applicable for all situations has motivated our present work.
37 The present work is an extended version of the fluid and kinetic
38 plasma dispersion relation solver BO code [1–3].

2. Equations to solve

39 In this work, we use cylindrical coordinates (r, ϕ, z) . The wave
40 vector variables are chosen as $(k_r, n_\phi = rk_\phi, k_z)$. The coordinate
41 relations are $x = r \cos \phi$, $y = r \sin \phi$, $k_x = k_r \cos \phi - \frac{n_\phi}{r} \sin \phi$ and
42 $k_y = k_r \sin \phi + \frac{n_\phi}{r} \cos \phi$. Note that the canonical coordinate for ϕ
43 is n_ϕ , not k_ϕ . If we use k_ϕ as a coordinate, the ray tracing equation
44 expressions would be more complicated, cf., Ref. [11].

2.1. Ray tracing equations in cylindrical coordinates

45 Performing the coordinate transformation from $(x, y, z, k_x, k_y,$
46 $k_z)$ to $(r, \phi, z, k_r, n_\phi, k_z)$, we can have

$$47 \frac{dr}{d\tau} = \frac{\partial D}{\partial k_r}, \quad \frac{d\phi}{d\tau} = \frac{\partial D}{\partial n_\phi}, \quad \frac{dz}{d\tau} = \frac{\partial D}{\partial k_z}, \quad (4)$$

$$48 \frac{dk_r}{d\tau} = -\frac{\partial D}{\partial r}, \quad \frac{dn_\phi}{d\tau} = -\frac{\partial D}{\partial \phi}, \quad \frac{dk_z}{d\tau} = -\frac{\partial D}{\partial z}, \quad (5)$$

49 with

$$50 \frac{dt}{d\tau} = -\frac{\partial D}{\partial \omega}, \quad (6)$$

51 Usually, the dispersion relation (3) is written as $D = D(\omega, k_\parallel, k_\perp^2) =$
52 0. Here, the parallel wave vector $k_\parallel = \mathbf{k} \cdot \mathbf{b} = \frac{1}{B} (k_r B_r + k_z B_z +$
53 $\frac{n_\phi}{r} B_\phi)$ is defined from the magnetic field \mathbf{B} , and $k_\perp^2 = k^2 - k_\parallel^2,$
54 $B = B(r, z) = \sqrt{B_r^2 + B_z^2 + B_\phi^2}, k^2 = k_r^2 + k_z^2 + \frac{n_\phi^2}{r^2}.$

55 We consider axisymmetric configurations, i.e., $\frac{\partial D}{\partial \phi} = 0$. We need
56 to calculate the ray tracing equation from $(r, \phi, z, k_r, n_\phi, k_z)$ to
57 $(r, \phi, z, k_\parallel, k_\perp^2, \alpha)$ with $\frac{\partial D}{\partial \alpha} = 0$, where α is the angle relevant to
58 two perpendicular wave vectors and can be omitted here since the
59 cold and hot dispersion relations D used in the present work are
60 function of k_\parallel and k_\perp but not α . We obtain

$$61 \frac{\partial D}{\partial k_r} \Big|_{r, \phi, z, n_\phi, k_z} = 2 \left(\frac{\partial D}{\partial k_\parallel^2} - \frac{\partial D}{\partial k_\perp^2} \right) k_\parallel \frac{B_r}{B} + 2 \frac{\partial D}{\partial k_\perp^2} k_r, \quad (7)$$

$$62 \frac{\partial D}{\partial n_\phi} \Big|_{r, \phi, z, k_r, k_z} = 2 \left(\frac{\partial D}{\partial k_\parallel^2} - \frac{\partial D}{\partial k_\perp^2} \right) k_\parallel \frac{B_\phi}{rB} + 2 \frac{\partial D}{\partial k_\perp^2} \frac{n_\phi}{r^2}, \quad (8)$$

$$63 \frac{\partial D}{\partial k_z} \Big|_{r, \phi, z, k_r, n_\phi} = 2 \left(\frac{\partial D}{\partial k_\parallel^2} - \frac{\partial D}{\partial k_\perp^2} \right) k_\parallel \frac{B_z}{B} + 2 \frac{\partial D}{\partial k_\perp^2} k_z, \quad (9)$$

$$64 \frac{\partial D}{\partial r} \Big|_{\phi, z, k_\parallel, k_\perp^2, \alpha} = \frac{\partial D}{\partial r} \Big|_{\phi, z, k_r, n_\phi, k_z} + 2 \left(\frac{\partial D}{\partial k_\parallel^2} - \frac{\partial D}{\partial k_\perp^2} \right) k_\parallel \frac{\partial k_\parallel}{\partial r} - 2 \frac{\partial D}{\partial k_\perp^2} \frac{n_\phi^3}{r^3} \quad (10)$$

$$65 \frac{\partial D}{\partial \phi} \Big|_{r, z, k_r, n_\phi, k_z} = 0, \quad (11)$$

$$66 \frac{\partial D}{\partial z} \Big|_{r, \phi, k_r, n_\phi, k_z} = \frac{\partial D}{\partial z} \Big|_{\phi, z, k_\parallel, k_\perp^2, \alpha} + 2 \left(\frac{\partial D}{\partial k_\parallel^2} - \frac{\partial D}{\partial k_\perp^2} \right) k_\parallel \frac{\partial k_\parallel}{\partial z}, \quad (12)$$

67 where

$$68 \frac{\partial k_\parallel}{\partial r} = -\frac{k_\parallel}{B} \frac{\partial B}{\partial r} + \frac{1}{B} \left(k_r \frac{\partial B_r}{\partial r} + k_z \frac{\partial B_z}{\partial r} + \frac{n_\phi}{r} \frac{\partial B_\phi}{\partial r} - \frac{B_\phi n_\phi}{r^2} \right), \quad (13)$$

$$69 \frac{\partial k_\parallel}{\partial z} = -\frac{k_\parallel}{B} \frac{\partial B}{\partial z} + \frac{1}{B} \left(k_r \frac{\partial B_r}{\partial z} + k_z \frac{\partial B_z}{\partial z} + \frac{n_\phi}{r} \frac{\partial B_\phi}{\partial z} \right). \quad (14)$$

2.2. Ray tracing equations for cold plasma dispersion relation

70 The cold plasma dispersion relation is

$$71 F(\omega, k_\parallel^2, k_\perp^2) = \varepsilon_1 \frac{k_\perp^4 c^4}{\omega^4} - \left[(\varepsilon_1 + \varepsilon_3) \left(\varepsilon_1 - \frac{k_\parallel^2 c^2}{\omega^2} \right) - \varepsilon_2^2 \right] \frac{k_\perp^2 c^2}{\omega^2} + \varepsilon_3 \left[\left(\varepsilon_1 - \frac{k_\parallel^2 c^2}{\omega^2} \right)^2 - \varepsilon_2^2 \right] = 0, \quad (15)$$

72 where

$$73 \varepsilon_1 = 1 - \sum_s \frac{\omega_{ps}^2}{\omega^2 - \omega_{cs}^2}, \quad \varepsilon_2 = \sum_s \frac{\omega_{cs}}{\omega} \frac{\omega_{ps}^2}{\omega^2 - \omega_{cs}^2},$$

$$74 \varepsilon_3 = 1 - \sum_s \frac{\omega_{ps}^2}{\omega^2}, \quad (16)$$

$$75 \mathbf{n} = \frac{\mathbf{k}c}{\omega}, \quad \omega_{cs} = \frac{q_s B}{m_s}, \quad \omega_{ps} = \sqrt{\frac{n_{s0} q_s^2}{\epsilon_0 m_s}}, \quad c = \frac{1}{\sqrt{\mu_0 \epsilon_0}}. \quad (17)$$

76 The derivatives for F can be readily written out explicit, i.e., $\frac{\partial F}{\partial k_\perp^2},$
77 $\frac{\partial F}{\partial k_\perp^2}, \frac{\partial F}{\partial r} \Big|_{\phi, z, k_\parallel, k_\perp^2, \alpha}, \frac{\partial F}{\partial z} \Big|_{r, \phi, k_\parallel, k_\perp^2, \alpha}$ and $\frac{\partial F}{\partial \omega}$, which are not shown
78 here.

79 We need the 2D equilibrium profiles $B_r(r, z), B_z(r, z), B_\phi(r, z),$
80 $B(r, z), n_{s0}(r, z)$ and their first order derivate $\partial/\partial r$ and $\partial/\partial z$.

We should note that the cold plasma dispersion relation Eq. (15) is singular at cyclotron resonant position of species $s = a$, say, if $\omega \simeq \omega_{c,s=a}$. This singularity is first order to $Y_a = 1 - \omega_{c,s=a}^2/\omega^2$, thus we can multiple Eq. (15) to define a new dispersion relation $G(\omega, k_{\parallel}^2, k_{\perp}^2) = Y_a F(\omega, k_{\parallel}^2, k_{\perp}^2)$ in the code, which is similar to the treatment in GENRAY [4]. One should also be careful that we do not use $G^{(n)}(\omega, k_{\parallel}^2, k_{\perp}^2) = Y_a^n F(\omega, k_{\parallel}^2, k_{\perp}^2)$ ($n \geq 2$), which will cause the group velocity vanish at resonant position. For cases with resonant singularity of more than one species at the same position, we should make sure the singularity have been removed for all species.

It should be noted that the above mathematical formulation is pertinent to both open and closed field line plasmas, and therefore the equations are applicable for both. Hence, the above equations can be used for various magnetized plasma configurations.

2.3. Wave absorption equation using hot kinetic plasma dispersion relation

Since the drift bi-Maxwellian distribution function may lead to unstable modes with imaginary part of wave frequency be positive, i.e., wave absorbs energy from particles, we only use the Maxwellian distribution hot kinetic dispersion relation for wave heating in the present version of BORAY. The non-relativistic dispersion tensor is standard, cf., [2].

For weak damping approximation with $\omega_i \ll \omega_r$ and $\mathbf{k}_i \ll \mathbf{k}_r$, for $D(\omega, \mathbf{k}) = D_r(\omega, \mathbf{k}) + iD_i(\omega, \mathbf{k}) = 0$, $D_i \ll D_r$, we have $D_r(\omega_r, \mathbf{k}_r) = 0$ and

$$i \left[\frac{\partial D_r(\omega_r, \mathbf{k}_r)}{\partial \omega_r} \omega_i + D_i(\omega_r, \mathbf{k}_r) \right] \simeq 0, \quad (18)$$

$$i \left[\frac{\partial D_r(\omega_r, \mathbf{k}_r)}{\partial \mathbf{k}_r} \mathbf{k}_i + D_i(\omega_r, \mathbf{k}_r) \right] \simeq 0, \quad (19)$$

we have

$$\mathbf{k}_i = - \frac{D_i}{\partial D_r / \partial \mathbf{k}_r}, \quad \omega_i = - \frac{D_i}{\partial D_r / \partial \omega_r}, \quad (20)$$

$$\mathbf{k}_i = \frac{\partial D_r / \partial \omega_r}{\partial D_r / \partial \mathbf{k}_r} \omega_i = - \frac{\omega_i}{\partial \omega / \partial \mathbf{k}_r} = - \frac{\omega_i}{\mathbf{v}_g}, \quad (21)$$

So the wave damping caused wave intensity $P(s)$ along the trajectory can be calculated from either \mathbf{k}_i or ω_i , due to

$$P(s) = P_0 \cdot e^{-2 \int_0^s \mathbf{k}_i \cdot d\mathbf{r}} = P_0 \cdot e^{-2 \int_0^t \omega_i dt}.$$

One can use Eq. (20) to calculate ω_i when the weak damping assumption is valid. In BORAY, we choose to calculate the complex $\omega = \omega_r + i\omega_i$ more accurately along the ray, since that usually the kinetic ω_r may deviate from initial wave frequency ω_0 , especially when we use the cold plasma dispersion relation instead of the kinetic one to calculate the ray trajectory. The BO code [1-3] is convenient to calculate the ω for given real \mathbf{k} for either kinetic or fluid plasma dispersion relations. So, we succeed the corresponding modules of BO to calculate the kinetic absorption in the present ray tracing code. Hence, we named the present code as BO-RAY (or, BORAY) as a branch of BO family.

To calculate the absorption ratio from different species, for simplicity, we keep only the temperature of that species unchanged and set the temperatures of other species to be cold.

3. Benchmarks and applications

In this section, to show the accuracy and capability of BORAY, we compare it with other ray tracing code, particle simulation and experiments. If not specialized, the tokamak and ST equilibria in the following examples are obtained from EFIT [12] outputs of

Table 1

BORAY benchmark and application examples, for varies wave frequencies and varies configurations, with numerical MHD equilibria (default), 3-fluid equilibrium (Fig. 8) and analytical MHD equilibrium (Fig. 9).

Configuration (Field Lines)	Tokamak (Closed)	ST (Both)	FRC (Both)	Mirror (Open)
B_ϕ	$\neq 0$	$\neq 0$	$= 0$	$= 0$
ECW (O&X)	Fig. 1	Fig. 8 (3-fluid eq.)		
LHW	Fig. 2			Fig. 6
Helicon	Fig. 3			
HHFW			Fig. 5	
ICW		Fig. 4, Fig. 9 (analy. eq.)		Fig. 7

corresponding configurations. All the examples in this section are summarized in Table 1, which are obtained by BORAY under a unified theoretical model and numerical code as described in Sec. 2, i.e., we do not need to choose different models for different examples. The only differences between different examples are the input magnetic fields, densities and temperatures profiles, and the initial wave frequency, position and wave vector.

In the present version of BORAY code, we do the calculations with three steps. Firstly, we use cold plasma model to solve the ray trajectory $(r, \phi, z, k_r, n_\phi, k_z)$ with fixed initial wave frequency ω_0 as described in subsections 2.1 and 2.2. Secondly, along the ray we use $(r, \phi, z, k_r, n_\phi, k_z)$ as the input of the cold plasma model to solve the $\omega(t)$ to check whether $\omega(t) = \omega_0$, i.e., to make sure the ray tracing equation is solved accurately. Thirdly, along the ray we use $(r, \phi, z, k_r, n_\phi, k_z)$ as the input of the kinetic plasma model to solve the $\omega(t) = \omega_r + i\omega_i$, and use ω_i to calculate the absorption/heating as described in subsection 2.3. Here, the kinetic ω_r in the third step may be deviated from initial wave frequency ω_0 .

3.1. Tokamak and ST ECW, LHW and ICW

In this subsection, we show the benchmarks between BORAY and GENRAY for several standard tokamak and ST cases, including the frequency from high to low, i.e., ECW X-mode and O-mode, LHW, helicon wave, and ICW.

Fig. 1 shows the comparison of BORAY and GENRAY for EAST tokamak 100 GHz ECW X-mode and O-mode, with central magnetic field $B_0 = 1.78T$, major radius $R_0 = 1.88$ m, safety factor $q_0 = 1.5$, density $n_{e0} = 5 \times 10^{19} \text{ m}^{-3}$ and temperature $T_{e0} = T_{i0} = 500$ eV.

Fig. 2 shows the comparison of BORAY and GENRAY for EAST tokamak 2.45 GHz LHW for the same equilibrium magnetic fields as in Fig. 1, but different densities and temperatures, $n_{e0} = 1 \times 10^{19} \text{ m}^{-3}$ and $T_{e0} = T_{i0} = 200$ eV.

Fig. 3 shows the comparison of BORAY and GENRAY for HL-2M tokamak 476 MHz helicon wave, with central magnetic field $B_0 = 1.76T$, major radius $R_0 = 1.85$ m, safety factor $q_0 = 0.98$, density $n_{e0} = 6.42 \times 10^{19} \text{ m}^{-3}$, $n_{D+0} = 5.39 \times 10^{19} \text{ m}^{-3}$, $n_{C+60} = 0.17 \times 10^{19} \text{ m}^{-3}$ and temperature $T_{e0} = 5.60$ keV, $T_{D+0} = T_{C+60} = 4.78$ keV.

Fig. 4 shows the comparison of BORAY and GENRAY for EXL-50 spherical tokamak 5 MHz ICW, with central magnetic field $B_0 = 0.26T$, major radius $R_0 = 0.89$ m, safety factor $q_0 = 10.9$, density $n_{e0} = 5.0 \times 10^{18} \text{ m}^{-3}$ and temperature $T_{e0} = 200$ eV and $T_{i0} = 50$ eV.

In all these above benchmark cases, both ray trajectories and power absorptions agree well. Some differences may come from numerical error or slightly different models implemented in the two codes. For examples, we only include collisionless damping in our model, whereas GENRAY includes also collisional damping for LHW. We carry out analysis to check validity of BORAY results. For example, in Fig. 3(e), we show the ω_r along the ray, which are solved from the cold and kinetic dispersion relations with the cold

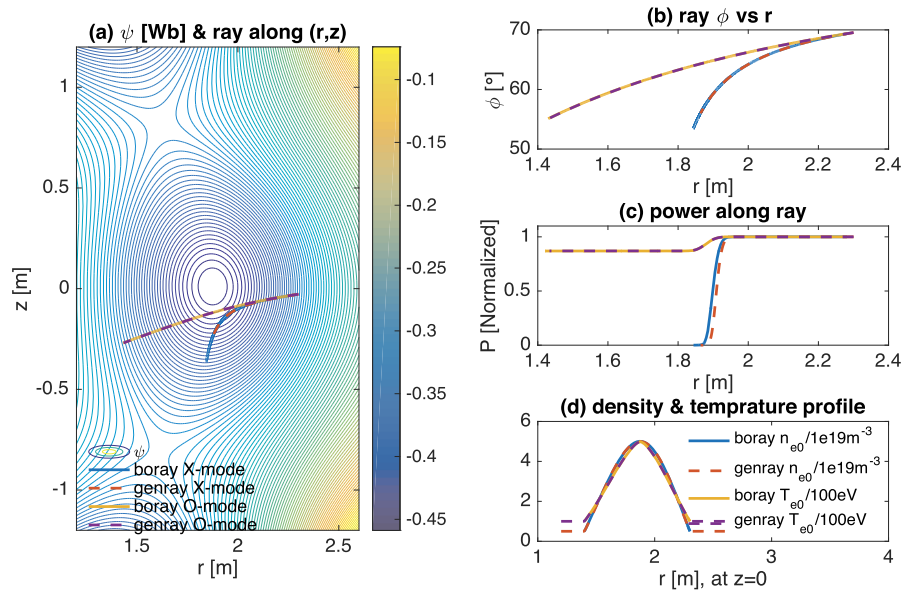


Fig. 1. Comparison of BORAY and GENRAY for EAST tokamak 100 GHz ECW O and X modes. Both ray trajectories and power absorptions agree well. (For interpretation of the colors in the figure(s), the reader is referred to the web version of this article.)

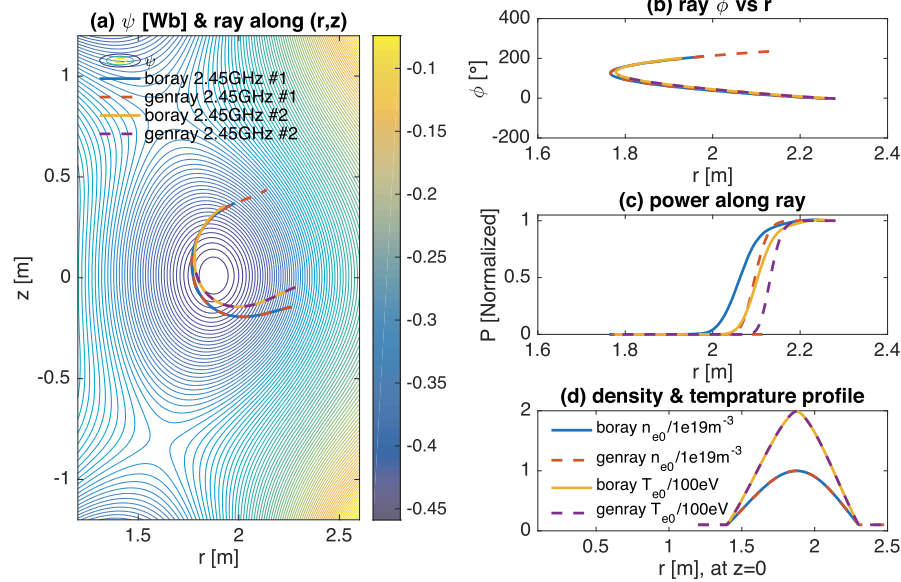


Fig. 2. Comparison of BORAY and GENRAY for EAST tokamak 2.45 GHz LHW. Ray trajectories agree well. However, GENRAY damping early than BORAY for power absorptions, which may due to different absorption models used in the two codes.

plasma ray tracing output k along the ray. We see that the cold plasma ω_r is almost identical to the given input wave frequency $\omega_0 = 2\pi f$, which means that the cold plasma ray tracing equation is solved accurately in BORAY. The deviation of kinetic ω_r to ω_0 implies that the cold plasma assumption for the ray tracing may not be accurate for this case. However, the $\omega_i/\omega_r \simeq 0.01$ means that the weak damping assumption still holds.

3.2. FRC high harmonic fast wave

Since BORAY does not use flux coordinates, it can support both closed and open field lines plasmas equally as default. We firstly show the result for FRC case. Fig. 5 shows C2-U FRC 7 MHz High Harmonic FW (HHFW) simulation results, which is similar to the GENRAY-C results in Ref. [13], i.e., the absorption can be 100%

and most power can be deposited inside the closed flux surface for optimized wave parameters. The equilibrium is generated by GSEQ-FRC [14] using similar parameters as in Ref. [13], with axis magnetic field $B(0, 0) = -0.05T$, major radius $R_0 = 0.35$ m, central density $n_{e0} = 2.4 \times 10^{19} \text{ m}^{-3}$ and temperature $T_{e0} = 150$ eV and $T_{D+10} = 800$ eV.

3.3. Mirror LHW and ICW

Here, we show the capability of BORAY for mirror configuration. Fig. 6 shows mirror 160 MHz LHW simulation results, which is close to the three dimensional (3D) electromagnetic particle-in-cell (PIC) simulations results in Ref. [17] as shown in Fig. 6(b) for both the ray trajectories and turning points. Here, the initial antenna $k_z = 16.3 \text{ m}^{-1}$. Note that the density is given as

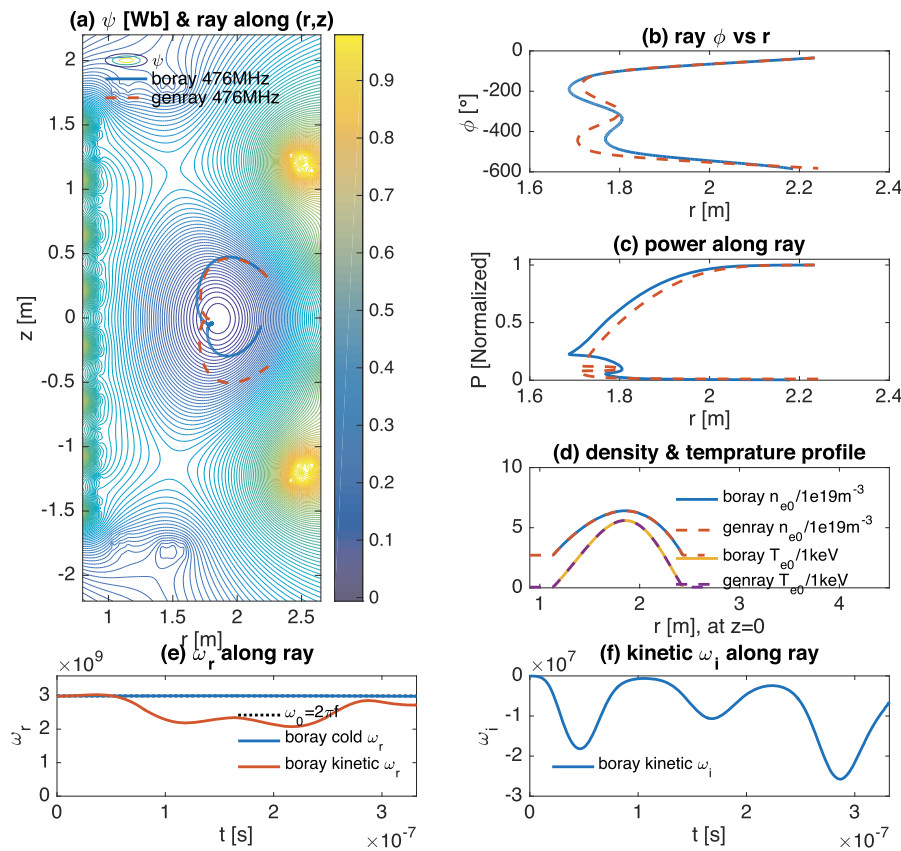


Fig. 3. Comparison of BORAY and GENRAY for HL-2M tokamak 476 MHz helicon wave [16]. Ray trajectories and power absorptions roughly agree. The difference may come from the numerical errors in GENRAY, since less than 200 points is used along the ray in GENRAY output.

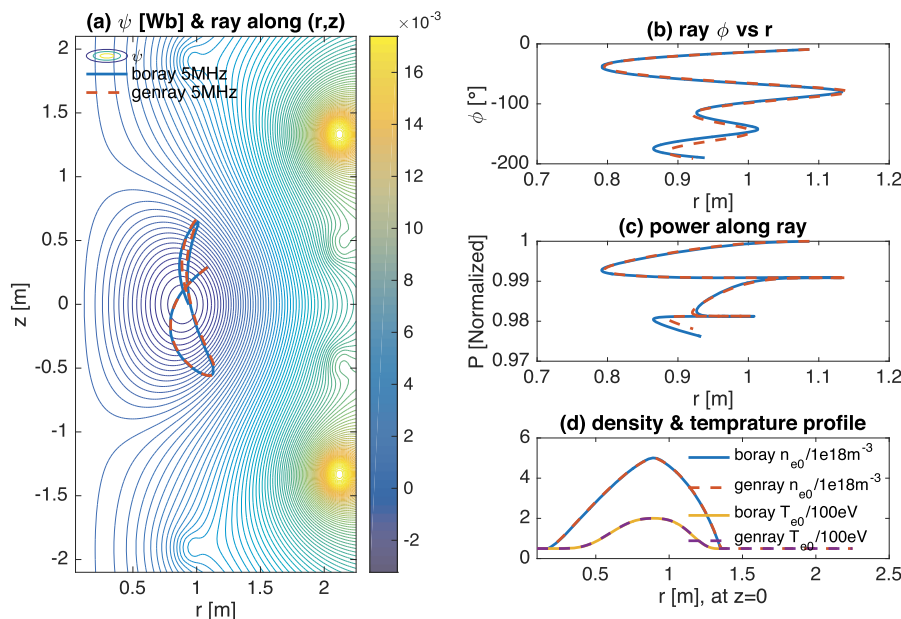


Fig. 4. Comparison of BORAY and GENRAY for EXL-50 spherical tokamak 5 MHz ICW. Both ray trajectories and power absorptions agree well. The slight difference may come from numerical error of time push or grid interpolation.

$n_{s0} = n_0 e^{-\frac{r^2}{2\sigma^2}}$, which is not set as function of magnetic flux. Here, $n_0 = 1 \times 10^{18} \text{ m}^{-3}$ and $\sigma = 0.045 \text{ m}$. Temperature is set as constant for both electrons and H ions, $T_{e0} = T_{H0} = 460 \text{ eV}$. More detailed comparisons can be found in Ref. [17].

Fig. 7 shows KMAX mirror 750 kHz ICW simulation results, which is close to the results in Ref. [22] of ICRF experiment,

i.e., absorption rate >40%. Initial wave parameters $(r, \phi, z, k_r, k_z) = (0.2, 0, 0.9, 90.2, -1, -8)$. Note that the summation of ion and electron damping rates is not equal to the total damping rate, which is probably due to the violation of weak damping approximation or that the effects of different species are not independent.

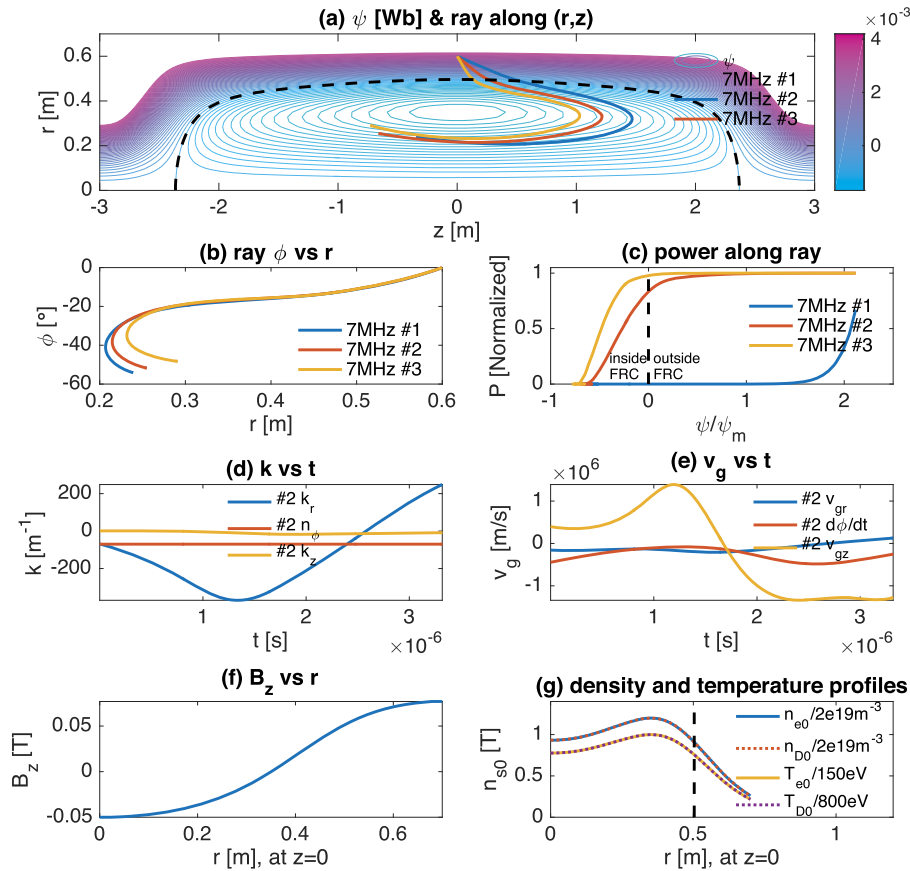


Fig. 5. C2-U FRC 7 MHz HHFW simulation results, which is similar to the results in Ref. [13], i.e., the absorption can be 100% and most power can be deposited inside the closed flux surface for optimized wave parameters.

3.4. ST ECW under multi-fluid equilibrium

In some STs, such as QUEST [19] and EXL-50 [20], the energetic (high energy) electrons (>10 keV) are important component. Ref. [18] provides a multi-fluid equilibrium model for EXL-50. Here, we show the capability of BORAY for this equilibrium configuration. Fig. 8 shows the EXL-50 spherical tokamak 28 GHz ECW O&X-modes under three-fluid equilibrium with central magnetic field $B_0 = 0.36T$, major radius $R_0 = 0.63$ m, safety factor $q_0 \approx 10$, maximum densities $n_{H^+} = 9.0 \times 10^{17} m^{-3}$, $n_{el} = 8.8 \times 10^{17} m^{-3}$, $n_{eh} = 1.76 \times 10^{16} m^{-3}$ and temperatures $T_{H^+} = 38$ eV, $T_{el} = 417$ eV and $T_{eh} = 313$ keV. The low density ($\sim 2\%$) high energy electrons (eh) contribute most of the power absorption, whereas the absorption from H^+ ions and low energy thermal electrons (el) are negligible. We obtain the three fluid equilibrium profiles for both inside and outside the last closed flux surface (LCFS) from the model in Ref. [18] for EXL-50 shot#6935 $t=4.45$ s, with total plasma current $I_p = 120$ kA. We also see that the X-mode have better absorption than O-mode, and the second order $2\omega_{ce}$ resonant is also stronger than that of O-mode. These energetic electron effects are similar to the recently reported [21] QUEST experimental and theoretical analysis results. We can also see from Fig. 8 (b) that some amount ($\sim 5\%$) of the wave absorption is outside the LCFS before the wave propagates to the closed field line region.

3.5. Comparison of ST ICW under numerical and analytical equilibria

Since numerical equilibrium may not always be easily available, we also provide analytical equilibrium in BORAY code. We are interested to quantify how the characteristics of wave propagation and value of absorption differ between cases of numerically reconstructed and analytical equilibria. Fig. 9 shows the comparison of

EXL-50 spherical tokamak 4.5 MHz ICW for numerical and analytical MHD equilibria, with three species, i.e., electrons, H^+ ions and 5% He^{2+} minority ions. The numerical equilibrium parameters are $B_0 = 0.32T$, major radius $R_0 = 0.64$ m, safety factor $q_0 = 1.6$, density $n_{e0} = 5.5 \times 10^{18} m^{-3}$ and temperature $T_{e0} = 200$ eV and $T_{i0} = 50$ eV. The construction of analytical equilibrium is described in Appendix B, with other model parameters $R_x = 0.17$ m, $E = 1.5$, $\tau = 0.8$, $L_{ns} = 0.9$ and $L_{ts} = 0.8$ for the present case. Both ray trajectories and power absorptions are similar for the numerical and analytical equilibria. For both cases, the CPU runtime of ray tracing are in seconds for 10000 time step points. The numerical equilibrium case (3s) is slightly faster than the analytical equilibrium case (7s). For this case, most power is absorbed by electrons and fundamental Ω_{cH^+} resonant, with also slight $2\Omega_{cHe^{2+}}$ resonant as can be seen from the damping rate sub-figures (e)&(f). Hence, if numerical equilibrium is not available, one can use the analytical equilibrium model in the code to do the calculations, since they can yield similar results.

4. Summary and discussion

A new plasma wave ray tracing code BORAY (<https://github.com/hsxie/boray>) has been developed for axisymmetric configurations to support both closed and open field lines plasma configurations. The code shows good agreement with GENRAY code for tokamak and ST cases of ECW, LHW, helicon wave and ICW, and also agrees well with 3D PIC simulation of LHW in mirror machine, and agrees with GENRAY-C for HHFW in FRC, and ICW for KMAX mirror experiment. Thus, it can be expected that BORAY can have wide application for the plasma wave propagation and heating studies and especially to help the design of the wave

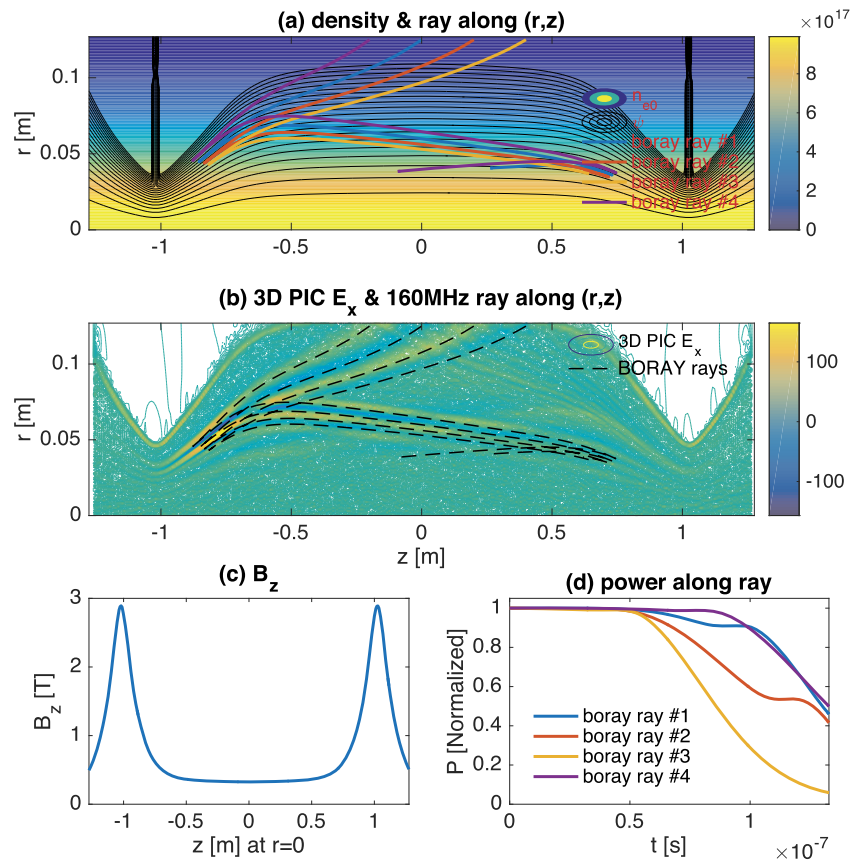


Fig. 6. Mirror 160 MHz LHW simulation results, which is close to the results in Ref. [17] of 3D PIC simulations results of the electric field, i.e., the ray trajectories from BORAY are just along where the electric field are strong in PIC results (b). The power absorptions (d) are also similar, i.e., the wave is almost decayed away before reaching the second turning point.

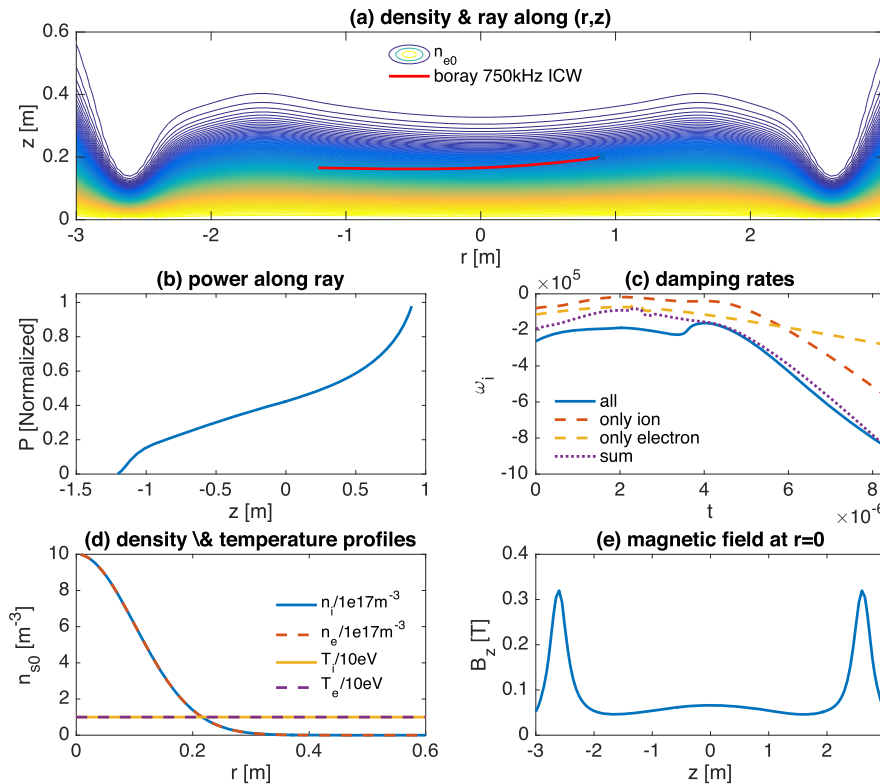


Fig. 7. KMAX mirror 750 kHz ICW simulation results, which is close to the results in Ref. [22] of ICRF experiment, i.e., absorption rate >40%.

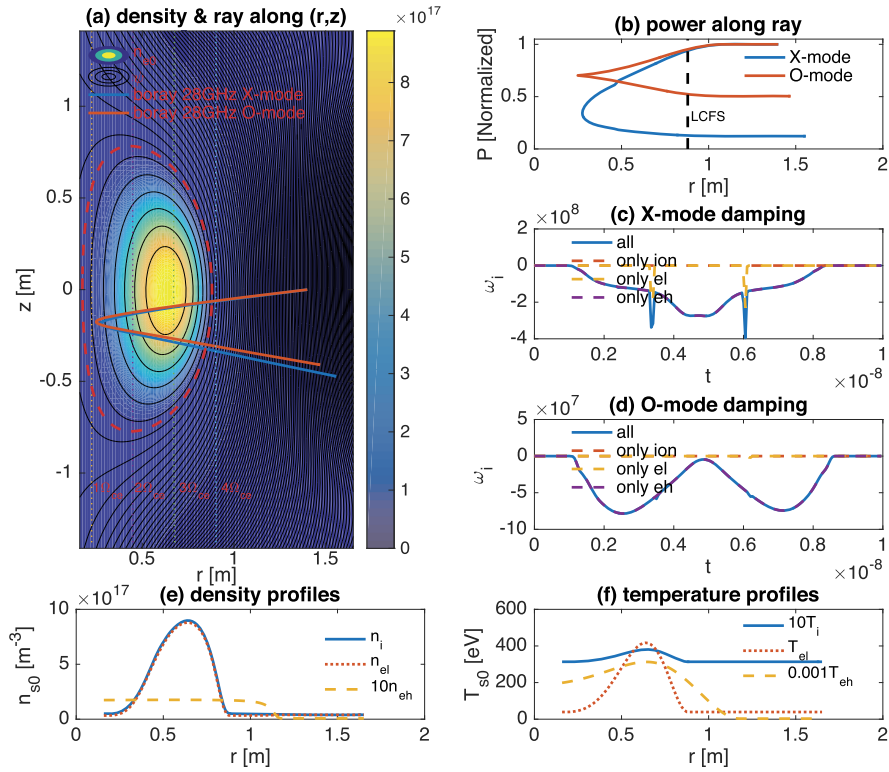


Fig. 8. EXL-50 spherical tokamak 28 GHz ECW O&X-modes, with three-fluid equilibrium. The high energy electrons (*eh*) contribute most of the power absorption, whereas the absorption from ions and low energy electrons (*el*) are negligible.

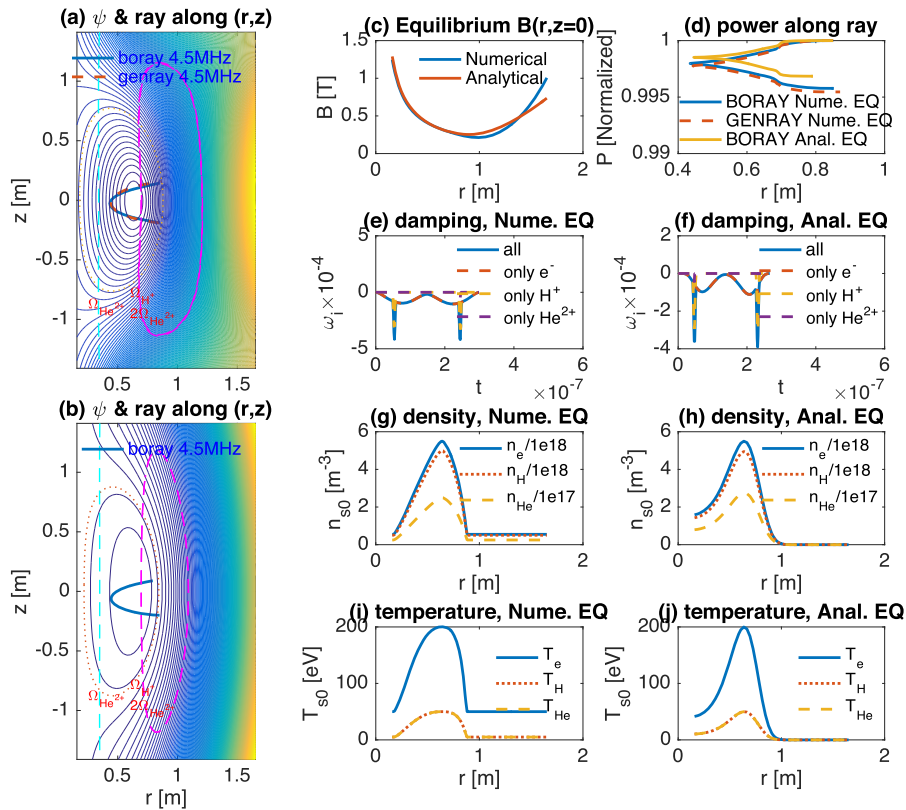


Fig. 9. Comparison EXL-50 spherical tokamak 4.5 MHz ICW for numerical and analytical MHD equilibria, with three species, i.e., electrons, H^+ ions and 5% He^{2+} minority ions. Both ray trajectories and power absorptions are similar.

heating system to choose the wave parameters. The code works for both numerical and analytical equilibria. However, we should also remind that although the ray tracing can give numerical results for low frequency waves, the user should always note that the results may not be valid when the wave length is not shorter than the scale length of medium, for which cases, full wave [23] studies are usually required. A valid example of ray tracing results by comparing with full wave simulation of HHFW can be found at Ref. [24]. Future works can include relativistic and collisional effects and calculating the current driven. Adding nonuniform at ϕ direction could be useful as well, such as to support ripple effects in tokamaks, and effects of drift wave turbulence. Considering that the present scheme is applicable to only the waves close to the cold plasma dispersion relation, modifying the cold plasma ray tracing model to kinetic dispersion relation to support electron and ion Bernstein waves could also be an important future topic, which we demonstrate at Ref. [25]. An improved model is also required to calculate the absorption ratio from different species more accurately.

Declaration of competing interest

The authors declare that they have no known competing financial interests or personal relationships that could have appeared to influence the work reported in this paper.

Acknowledgements

Discussion with Shao-dong Song, Guang-hui Zhu are acknowledged. We also thank Jiang-shan Zheng for providing the 3D PIC mirror LHW simulation data, and Wen-jun Liu for providing the three fluid equilibrium of EXL-50 spherical tokamak, and the Center for Computational Science and Engineering of Southern University of Science and Technology. We are grateful to Yu.V. Petrov and R.W. Harvey of CompX for introducing us the details of GENRAY code. This work is supported by the compact fusion project in ENN group.

Appendix A. More details of BORAY

Bi-linear interpolation is used for uniform (r, z) grids, which can be fast, and even can be faster than analytical equilibrium if we calculated the interpolation coefficients beforehand. In many tests, we find it is accurate enough. For wave absorption, we do not need calculate every point along the ray. Instead, we calculated the ray trajectory firstly with high accuracy, say ≥ 10000 time step

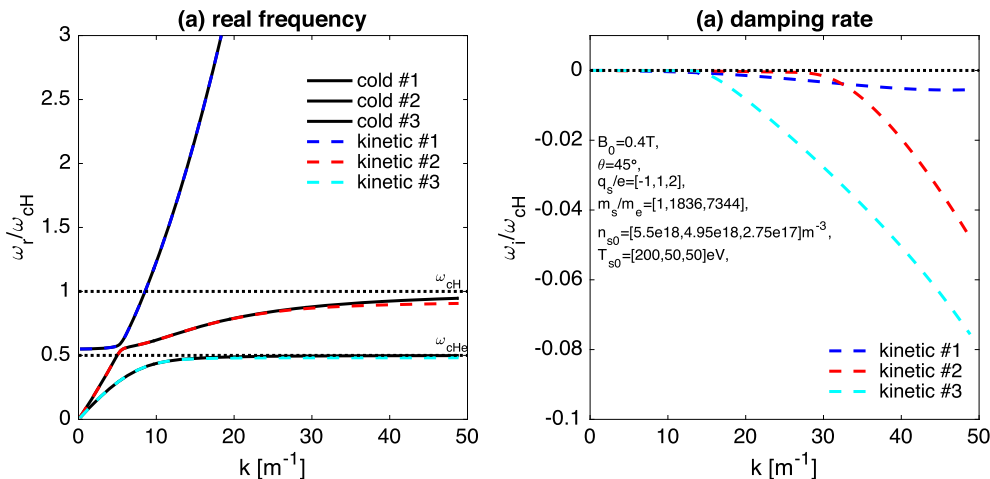


Fig. A.10. Waves in ICW range for the EXL-50 He^{2+} minority ions heating case. Solutions are calculated by the fluid and kinetic versions of BO [1].

Table A.2

Fluid and kinetic plasma waves and instabilities code BO family [1–3].

	Type	Names	References
BO family (open source)	dispersion relation ($\mathbf{k} \rightarrow \omega$)	PDRF, PDRK, BO, BO2.0	Xie14, 16,19,21
	ray tracing ($\omega \rightarrow \mathbf{k}$)	BORAY	Xie22 (this work)

points, and then select several points, say 200–1000 points, to calculate the damping rates, and then integral them to obtain the power absorption. SI units are used for all variables, except that the temperature unit is eV.

The user should generate the initial 2D (r, z) magnetic fields, densities and temperatures profile firstly and also give their derivatives to r and z . Also, the user should give the initial wave parameters, i.e., wave frequency $f = \omega/2\pi$ and $(r, \phi, z, k_r, \text{guess}, n_\phi, k_z)$. To make $D(\omega, \mathbf{k}) = 0$, BORAY calculate k_r from given n_ϕ and k_z . Multi- k_r may exist, the user can adjust k_r, guess to solve the corresponding k_r who wants. For examples, we use different k_r, guess to obtain X and O modes.

To analysis the wave feature in multi-species plasmas and to find the reasonable initial wave vector, the fluid and kinetic version of BO code can be useful, which can give all the wave frequency ω solutions for given wave vector \mathbf{k} at one time without the requirement of initial guess frequency and thus will not miss solutions. We show a typical ω vs. k figure in Fig. A.10 for ICRF minority heating parameter relevant to the case in Fig. 9. For this case, we can see that three branches exist in the ion cyclotron frequency range, and the kinetic correction to the cold plasma real frequency is small. Table A.2 summaries the role of each codes in BO family.

Appendix B. Analytical Solovév equilibrium for varies configurations

Analytical equilibrium can be useful for fast study the wave feature and can avoid the numerical interpolation error of numerical equilibrium from discrete grids. We construct an analytical Solovév equilibrium to include tokamak, spherical tokamak, FRC and mirror configuration in a same model, and which is also the solution of Grad-Shafranov MHD equilibrium equation.

The normalized equilibrium poloidal flux is [26]

$$\psi(r, z) = -rA_\phi = \frac{\psi_0}{R_0^4} \left\{ (r^2 - R_0^2)^2 + \frac{z^2}{E^2} (r^2 - R_x^2) \right\}$$

$$- \tau R_0^2 \left[r^2 \ln \left(\frac{r^2}{R_0^2} \right) - (r^2 - R_0^2) - \frac{(r^2 - R_0^2)^2}{2R_0^2} \right], \quad (\text{B.1})$$

where R_0 is major radius and the magnetic axis position $\psi(R_0, 0) = 0$. R_x , E and τ control the position of X-point, elongation and triangularity. The magnetic field are

$$B_r = -\frac{1}{r} \frac{\partial \psi}{\partial z} = -\frac{2\psi_0}{rR_0^4} \left[\frac{z}{E^2} (r^2 - R_x^2) \right], \quad (\text{B.2})$$

$$B_z = \frac{1}{r} \frac{\partial \psi}{\partial r} = \frac{2\psi_0}{R_0^4} \left\{ 2(r^2 - R_0^2) + \frac{z^2}{E^2} - \tau R_0^2 \left[\ln \left(\frac{r^2}{R_0^2} \right) - \frac{(r^2 - R_0^2)}{R_0^2} \right] \right\}. \quad (\text{B.3})$$

At X-point, $B_z(R_x, Z_x) = 0$, which gives

$$Z_x = E \sqrt{\tau R_0^2 \ln \left(\frac{R_x^2}{R_0^2} \right) + (2 + \tau)(R_0^2 - R_x^2)}. \quad (\text{B.4})$$

Toroidal magnetic field

$$B_\phi = \frac{B_0 R_0}{r}. \quad (\text{B.5})$$

Around magnetic axis ($z \rightarrow 0$, $r \rightarrow R_0$), we can have

$$\psi = 4\psi_0 \epsilon^2, \quad \epsilon \equiv \frac{r - R_0}{R_0} \ll 1, \quad \kappa \equiv \frac{2E}{\sqrt{1 - R_x^2/R_0^2}}. \quad (\text{B.6})$$

Thus poloidal magnetic field and safety factor around O-point is

$$B_p = 8 \frac{\psi_0}{R_0^2} \epsilon, \quad q_0 = \frac{r B_0}{R_0 B_p} = \frac{B_0 R_0^2}{8 \psi_0}, \quad (\text{B.7})$$

which gives

$$\psi_0 = \frac{B_0 R_0^2}{8 q_0}. \quad (\text{B.8})$$

The above model is very convenient to construct tokamak and spherical tokamak configurations.

To construct FRC configuration, we set $\tau = 0$, $R_x = 0$ and $B_\phi = 0$, which yields Hill-vortex equilibrium. And we set the magnetic $B_z(0, 0) = B_0$, which gives $\psi_0 = \frac{B_0 R_0^2}{4}$. The FRC model also holds for mirror configuration, we only need set further $R_0^2 < 0$. That is, the Eq. (B.1) can combine all the above several configurations in one model.

We construct the density and temperature profiles as

$$n_{s0}(r, z) = n_{s00} e^{-\frac{\psi}{\psi_x L_{ns}^2}}, \quad (\text{B.9})$$

$$T_{s0}(r, z) = T_{s00} e^{-\frac{\psi}{\psi_x L_{ts}^2}}, \quad (\text{B.10})$$

where n_{s00} and T_{s00} are density and temperature of species s at O-point, and L_{ns} and L_{ts} are normalized scaling length of their radial profiles, with $\psi_x \equiv \psi(R_x, Z_x)$. Thus, the derivatives are readily obtained, say

$$\frac{\partial n_{s0}}{\partial r} = -\frac{1}{\psi_x L_{ns}^2} n_{s0}(r, z) \frac{\partial \psi}{\partial r} = -\frac{r B_z}{\psi_x L_{ns}^2} n_{s0}, \quad (\text{B.11})$$

$$\frac{\partial n_{s0}}{\partial z} = -\frac{1}{\psi_x L_{ns}^2} n_{s0}(r, z) \frac{\partial \psi}{\partial z} = \frac{r B_r}{\psi_x L_{ns}^2} n_{s0}. \quad (\text{B.12})$$

The derivatives of magnetic field components are also readily obtained, and not shown here. One should also note that in ray tracing study, the equilibrium merely provides the magnetic configuration, and the density and temperature profiles are usually not set self-consistently.

References

- [1] H.S. Xie, Comput. Phys. Commun. 244 (2019) 343–371; H.S. Xie, R. Denton, J.S. Zhao, W. Liu, BO 2.0: plasma wave and instability analysis with enhanced polarization calculations, arXiv:2103.16014, 2021, <https://github.com/hsxie/bo/>.
- [2] H.S. Xie, Y. Xiao, Plasma Sci. Technol. 18 (2) (2016) 97, <https://doi.org/10.1088/1009-0630/18/2/01>, Update/bugs fixed at <http://hsxie.me/codes/pdrk/>, or <https://github.com/hsxie/pdrk/>.
- [3] H.S. Xie, Comput. Phys. Commun. 185 (2014) 670–675.
- [4] A.P. Smirnov, R.W. Harvey, The GENRAY ray tracing code, https://www.compcco.com/Genray_manual.pdf, <https://github.com/compcco/genray>, 2003.
- [5] Y. Peysson, J. Decker, L. Morini, Plasma Phys. Control. Fusion 54 (2012) 045003.
- [6] E. Mazzucato, I. Fidone, G. Granata, Phys. Fluids 30 (1987) 3745–3751.
- [7] D.B. Batchelor, R.C. Goldfinger, RAYS: a Geometrical Optics Code for EBT, ORNL/TM-6844, 1982.
- [8] M. Brambilla, Comput. Phys. Rep. 4 (1986) 71–93.
- [9] A. Esterkin, A. Piliya, Nucl. Fusion 36 (1996) 1501–1512.
- [10] A. Fukuyama, Integrated Tokamak Code: TASK, version 5, 20180117, Kyoto University.
- [11] B.D. McVey, Nucl. Fusion 19 (1979) 461.
- [12] L. Lao, H.S. John, R. Stambaugh, A. Kellman, W. Pfeiffer, Nucl. Fusion 25 (1985) 1611.
- [13] X. Yang, Y. Petrov, F. Ceccherini, A. Koehn, L. Galeotti, S. Dettrick, M. Binderbauer, the TAE Team, EPJ Web Conf. 157 (2017) 03065.
- [14] H.J. Ma, H.S. Xie, B.H. Deng, Y.K. Bai, S.K. Cheng, Y. Li, B. Chen, M. Tuszewski, H.Y. Zhao, J.Y. Liu, Nucl. Fusion 61 (2021) 086006.
- [15] A.G. Shalashov, E.D. Gospodchikov, O.B. Smolyakova, P.A. Bagryansky, V.I. Malygin, M. Thumm, Phys. Plasmas 19 (2012) 052503.
- [16] J.C. Li, X.T. Ding, J.Q. Dong, S.F. Liu, Plasma Phys. Control. Fusion 62 (2020) 095013.
- [17] J.S. Zheng, G.H. Zhu, J.S. Chen, Y.F. Zheng, J.Y. Xiao, X. Sun, G. Zhuang, H. An, D.X. Chen, X. Liu, F. Li, Nucl. Fusion 61 (2021) 126028.
- [18] A. Ishida, Y. Martin Peng, W.J. Liu, Phys. Plasmas 28 (2021) 032503.
- [19] T. Onchi, H. Idei, M. Fukuyama, D. Ogata, R. Ashida, T. Kariya, A. Ejiri, K. Matsuzaki, Y. Osawa, Y. Peng, S. Kojima, O. Watanabe, M. Hasegawa, K. Nakamura, K. Kuroda, R. Ikezoe, T. Ido, K. Hanada, N. Bertelli, M. Ono, A. Fukuyama, Phys. Plasmas 28 (2021) 022505.
- [20] Y.J. Shi, B. Liu, S.D. Song, Y.Y. Song, X.M. Song, B.W. Tong, S.K. Cheng, W.J. Liu, M.Y. Wang, T.T. Sun, D. Guo, S.J. Li, Y.Y. Li, B. Chen, X. Gu, J.Q. Cai, D. Luo, D. Banerjee, X. Zhao, Y.M. Yang, W.W. Luo, P.H. Zhou, Y. Wang, A. Ishida, T. Maekawa, M.S. Liu, B.S. Yuan, Y.-K. Martin, Peng and the EXL-50 team, Solenoid-free current drive via ECRH in EXL-50 spherical torus plasmas, arXiv:2104.14844, 2021.
- [21] M. Ono, N. Bertelli, H. Idei, K. Hanada, T. Onchi, S. Kojima, H. Elserafy, AIP Conf. Proc. 2254 (2020) 090001.
- [22] M. Liu, H.S. Yi, G.H. Zhu, Z.D. Yang, M.N. Lin, X. Sun, Phys. Plasmas 25 (2018) 082515.
- [23] M. Brambilla, Plasma Phys. Control. Fusion 41 (1999) 1–34.
- [24] G. Taylor, J.C. Hosea, C.E. Kessel, B.P. LeBlanc, D. Mueller, C.K. Phillips, E.J. Valeo, J.R. Wilson, P.M. Ryan, P.T. Bonoli, J.C. Wright, R.W. Harvey, Phys. Plasmas 19 (2012) 042501.
- [25] H.S. Xie, H.J. Ma, Y.K. Bai, Plasma waves accessibility diagrams: a tutorial to include the fluid and kinetic thermal effects, arXiv:2111.05669, 2021.
- [26] P. Helander, D. Sigmar, Collisional Transport in Magnetized Plasmas, Cambridge University Press, 2001, p. 292, Chapter 7.